Use of Pt and Boron-Doped Diamond Anodes in the Electrochemical Advanced Oxidation of Ponceau SS Diazo Dye in Acidic Sulfate Medium

Alexsandro Jhones dos Santos,[b] Carlos A. Martínez-Huitle,[b] Ignasi Sirés,[a] and Enric Brillas*[a]

The electrochemical degradation of 2.5 L of Ponceau SS diazo dye solution in acidic sulfate medium has been studied in a pre-pilot flow plant with a boron-doped diamond (BDD)/air-diffusion or Pt/air-diffusion cell connected to an annular photoreactor. The decolorization and mineralization was enhanced in the order: electrochemical oxidation with electrogenerated H_2O_2 < electro-Fenton < photoelectro-Fenton. The two former methods performed better with the BDD anode, whereas the latter yielded similar res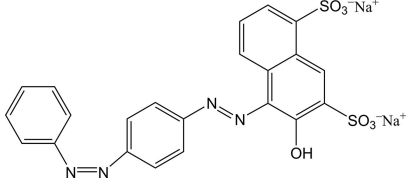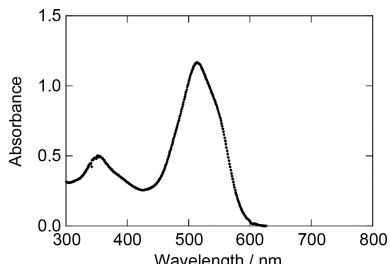ults for both anodes. From this, the use of less expensive active anodes such as Ti|Pt instead of non-active BDD for photo-assisted Fenton-based electrochemical processes is recommended. In all methods, increasing current density led to a greater degradation rate, but with lower mineralization current efficiency and higher energy consumption. Five primary aromatic products and four final carboxylic acids were detected, along with recalcitrant products poorly removed by hydroxyl radicals and UVA radiation.

1. Introduction

Acid azo dyes are mainly utilized in textile industries for dyeing of natural (silk, cotton, wool) and synthetic (rayon, acrylic, polyester) fibers.[1–4] They can also be used in leather, plastics, inks, and paints. These dyes are characterized by a high solubility in water because the azo group is linked to aromatic rings containing $-SO_3^-$ groups.[1,4] All around the world, a high number of industries discharges large volumes of wastewater containing up to 250 mg L^{-1} of dyes into the aquatic environment, causing a considerable impact in water bodies due to their increase in color and limited light penetration.[5] Moreover, acid azo dyes and their by-products present a large resistance to biodegradation and can cause negative effects to living beings, such as mutagenicity, carcinogenicity, and toxicity.[6–9] This is the case of Ponceau SS or Acid Red 150 (characteristics shown in Table 1), also employed as stain in biomedical applications, including hematology and histology. It has been documented that Ponceau SS is irritant to eyes and may alter lung functions giving rise to pneumoconiosis. Despite all these concerns, no previous work dealing with the removal of this diazo dye from wastewater has been reported yet.

Several electrochemical technologies[3,4] have shown larger ability for the remediation of water contaminated with azo dyes than classical technologies such as filtration,[7] adsorption,[10]

Table 1. Characteristics of Ponceau SS diazo dye.

|	
Chemical structure	(structure shown)
Chemical name	disodium 3-hydroxy-4-{2-[4-(2-phenyldiazen-1-yl)phenyl]diazen-1-yl}naphthalene-2,7-disulfonate
Chemical formula	$C_{22}H_{14}N_4Na_2O_7S_2$
Color Index number	27190
M [g mol^{-1}]	556.48
λ_{max} [nm]	514
UV/Vis spectrum	(spectrum shown)

and coagulation.[10,11] Electrocoagulation is one of the most typical electrochemical methods, in which a fraction of pollutants and their oxidation products can be coagulated with $Fe(OH)_n$ or $Al(OH)_3$ flocs originated from oxidation of sacrificial Fe or Al anodes, respectively. Nevertheless, this is mainly a phase separation method since organics are transferred to the sludge formed, which needs post-treatment.[3] More appropriate technologies for azo dyes removal are the electrochemical advanced oxidation processes (EAOPs), which involve the destruction of organics up to mineralization by the attack of reactive oxygen species (ROS) generated on site, like the strong

[a] Prof. I. Sirés, Prof. E. Brillas
Departament de Química Física
Facultat de Química, Universitat de Barcelona
Martí i Franquès 1–11, 08028 Barcelona, Spain
E-mail: brillas@ub.edu
[b] A. J. dos Santos, Prof. C. A. Martínez-Huitle
Instituto de Química
Universidade Federal do Rio Grande do Norte
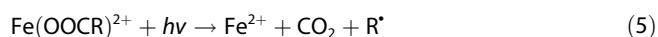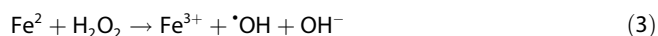Lagoa Nova – CEP 59.072-900, RN, Brazil

oxidant $^\bullet OH$.[4,11–15] In all the EAOPs, water oxidation at the anode M produces physisorbed $M(^\bullet OH)$ at high current by reaction (1) that attacks organic pollutants.[11,16–18] In anodic oxidation (AO), this is the only oxidant. If an adequate cathode to produce H_2O_2 by reduction of injected O_2 from reaction (2) is used as counterpart, the process is so-called AO with electro-generated H_2O_2 (AO-H_2O_2) and organics are not only attacked by $M(^\bullet OH)$, but also by weaker oxidants like H_2O_2 and its anodic oxidation product, hydroperoxyl radical ($HO_2^\bullet$).[15,19]

$$M + H_2O \rightarrow M(^\bullet OH) + H^+ + e^- \qquad (1)$$

$$O_{2(g)} + 2H^+ + 2e^- \rightarrow H_2O_2 \qquad (2)$$
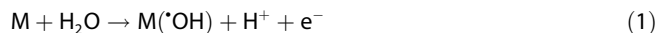
Good efficiencies for reaction (2) have been found by employing carbonaceous cathodes. Among them, materials such as graphite,[20] graphite felt,[21] carbon sponge,[22] carbon felt,[21,23–25] carbon nanotubes,[26,27] and carbon-polytetrafluoro-ethylene (PTFE) air-diffusion[28–30] electrodes have been utilized. On the other hand, it is well known that the anode material has remarkable influence on the oxidation power of AO and AO-H_2O_2.[4,18,21] An active anode like Pt produces low amounts of reactive $Pt(^\bullet OH)$ from reaction (1) because the strong Pt-$^\bullet OH$ interaction and low O_2-evolution overpotential facilitates its oxidation to yield the weaker "chemisorbed" PtO_x species, which favors the electrochemical conversion of organics into carboxylic acids.[21,31] The opposite behavior is accomplished for a non-active anode such as boron-doped diamond (BDD), in which organics become incinerated to CO_2 due to the high quantities of reactive $BDD(^\bullet OH)$ produced because of the larger overpotential required for O_2 evolution along with the very weak BDD-$^\bullet OH$ interaction.[31–33] At present, the BDD anode is considered the best material for these methods.

Recently, Fenton-based EAOPs have shown larger ability to remove azo dyes from wastewater.[28,29,34,35] In these processes, cathodically generated H_2O_2 is catalytically converted into $^\bullet OH$ by Fenton's reaction (3) upon the action of a small concentration of added Fe^{2+}.[36–38] This occurs in the electro-Fenton (EF) method, where $M(^\bullet OH)$ and $^\bullet OH$ are the main oxidants, with optimum pH near 3.[28,33,37] Reduction of Fe^{3+} to Fe^{2+} at the cathode propagates Fenton's reaction (3).[15,37,38] A modification of EF is photoelectro-Fenton (PEF), which involves the illumination of treated solution with UVA light.[4,39] This light can cause the quick photolysis of some products such as $Fe(OH)^{2+}$ by reaction (4), enhancing Fe^{2+} and $^\bullet OH$ production, along with that of final carboxylic acids via reaction (5).[40,41] When natural sunlight is utilized as free energy source, the process is so-called solar PEF (SPEF), which is much more cost-effective for wastewater treatment.[29,42,43]

$$Fe^2 + H_2O_2 \rightarrow Fe^{3+} + {}^\bullet OH + OH^- \qquad (3)$$

$$Fe(OH)^{2+} + h\nu \rightarrow Fe^{2+} + {}^\bullet OH \qquad (4)$$

$$Fe(OOCR)^{2+} + h\nu \rightarrow Fe^{2+} + CO_2 + R^\bullet \qquad (5)$$

A limited number of papers has shown that the influence of the anode (active and non-active) over the performance of photo-assisted Fenton-based EAOPs to degrade organics is small because of the powerful photolytic action of UV radiation.[30,44] This differs from the results found for the AO process, where the non-active BDD anode presents much greater oxidation ability than the active ones. More research efforts are required to know if such behavior is also verified during the degradation of acid azo dyes since this represents a key factor for the viability and scale-up of the EAOPs at industrial scale.

This work presents a study on the decolorization and mineralization of Ponceau SS diazo dye solutions in acidic sulfate medium by means of AO-H_2O_2, EF, and PEF. The assays were made in a 2.5 L pre-pilot flow plant as a first approach, allowing the determination of the current efficiency and energy consumption. Aiming to clarify the role of the anode in each EAOP, an active Ti|Pt and a non-active BDD were used under comparable conditions. H_2O_2 was always supplied by a carbon-PTFE air-diffusion electrode. The effect of current density (j) on the performance of each process was examined. Gas chromatography-mass spectrometry (GC-MS) and high-performance liquid chromatography (HPLC) were utilized to detect the primary aromatic intermediates and final carboxylic acids, respectively.

2. Results and Discussion

2.1. Degradation of Ponceau SS using a Pt Anode

First, the ability of the pre-pilot flow plant to generate H_2O_2 with a Pt/air-diffusion cell was tested using 0.050 M Na_2SO_4 as background electrolyte at pH 3.0, 35 °C and $j=50$ mA cm^{-2}. Under these AO-H_2O_2 conditions, 15.1 mM H_2O_2 (33.8% efficiency) were accumulated at 360 min. The efficiency decreased over time, which can be ascribed to the anodic oxidation of this species to O_2 via $HO_2^\bullet$ as intermediate.[4,15] In the presence of 0.50 mM Fe^{2+} (EF conditions), a greater H_2O_2 decay was found, only achieving 4.3 mM by the concurrence of Fenton's reaction (3). When the solution was recirculated through the annular photoreactor containing a 160 W UVA lamp (PEF conditions), the drop of accumulated H_2O_2 was more pronounced, attaining 1.5 mM at 360 min, due to the acceleration of Fenton's reaction (3) induced by the photolytic reaction (4). These findings show that the amount of H_2O_2 generated in both Fenton-based EAOPs was high enough for maximum $^\bullet OH$ production.

Then, solutions with 0.19 mM Ponceau SS (50 mg L^{-1} of total organic carbon (TOC)) were prepared under the above conditions to be degraded by AO-H_2O_2, EF and PEF at j values of 25, 50, and 100 mA cm^{-2} for 360 min in order to examine the role of oxidants. In EF and PEF, a catalytic concentration 0.50 mM of Fe^{2+} was added as optimal quantity.[41–43] A little change in solution pH was found in all these trials, showing a slight decrease to final pH 2.7–2.8 due to the formation of acidic by-products.
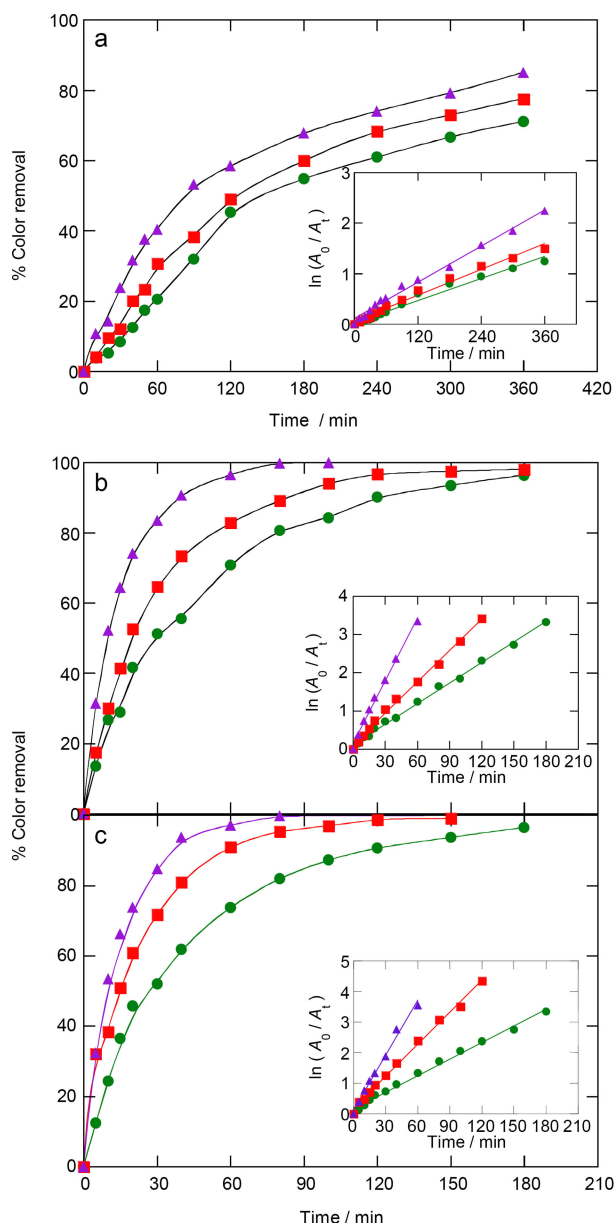
Figure 1. Decolorization efficiency vs. time for 2.5 L of 0.19 mM PCSS solution in 0.050 M Na_2SO_4 at pH 3.0 and 35 °C using a pre-pilot flow plant with a Pt/air-diffusion cell by a) AO-H_2O_2, b) EF with 0.50 mM Fe^{2+}, and c) PEF with 0.50 mM Fe^{2+}. Current density: 25 (●, green), 50 (■, red), and 100 mA cm^{-2} (▲, violet). Insets: Kinetic analysis assuming a pseudo-first-order decolorization reaction.

Figure 1a–c illustrates the change of percentage of color removal or decolorization efficiency for all these assays. This parameter was determined from the decay of absorbance (A) at the $\lambda_{max} = 514$ nm of Ponceau SS (Table 1) as follows:[28,34]

$$\% \text{Color removal} = \frac{A_0 - A_t}{A_0} 100 \qquad (6)$$

where A_0 denotes the initial absorbance and A_t that at time t. Two findings can be observed in Figure 1a–c. On the one hand, color removal was upgraded with increasing j, in agreement

with the higher rate of reactions (1) and (2) that yield greater amounts of H_2O_2 and Pt($^\bullet$OH), respectively, thus causing a quicker removal of the dye and its colored products. In addition, in EF and PEF the $^\bullet$OH production from Fenton's reaction (3) is accelerated by the rise of H_2O_2 content. On the other hand, it is evident that $^\bullet$OH generated in the latter two EAOPs decolorizes much more quickly the solution.

At $j = 100$ mA cm^{-2}, for example, color was reduced by 85.1% after 360 min of AO-H_2O_2, whereas the solution was completely decolorized at about 100 and 90 min in EF and PEF, respectively. This means that the decolorization power of EAOPs increased in the order: AO-$H_2O_2 \ll$ EF $\leq$ PEF. The superiority of PEF over EF can be accounted for by the extra $^\bullet$OH generation provided by photolytic reaction (4).

To gain a better insight into the decolorization rate of the above assays, the absorbance decays were analyzed considering that they obeyed a pseudo-first-order kinetics. The excellent linear correlations obtained are presented in the insets of Figure 1a–c, and the slope corresponded to the decolorization rate constant (k_{dec}). The k_{dec}-values thus found along with their R^2 are listed in Table 2. A look to this table corroborates the enhancement of k_{dec} as j was increased in each treatment, as well as the faster loss of color attained by EF and PEF compared to AO-H_2O_2. So, the k_{dec}-value was 9.2-fold and 10-fold higher for the two former processes at $j = 100$ mA cm^{-2}. This confirms the important oxidation role of $^\bullet$OH in the bulk because it is able to quickly destroy high quantities of Ponceau SS and its colored products.

Figure 2a–c depicts the TOC-time plots determined for the above tests. A progressive TOC removal along electrolysis time can be observed for each EAOP, which was enhanced when j was increased, according to the greater amounts of hydroxyl radicals generated, as stated above. However, unlike decolorization, the percentage of TOC removal increased in the order: AO-$H_2O_2 <$ EF $<$ PEF, with an evident rise for the PEF process due to the expected parallel photolysis of photoactive products upon UVA illumination, e.g., Fe(III)-carboxylate complexes via reaction (5). This tendency can also be deduced from the percentages of TOC removal collected in Table 2. As can be seen, the highest mineralization with 93.4% TOC reduction was achieved after 360 min of PEF at $j = 100$ mA cm^{-2}, a value 1.6-fold and 3.3-fold greater than those obtained for EF and AO-H_2O_2, respectively. This means that the photolytic action of UVA light is much more relevant on the multiple organic intermediates than on the parent diazo dye.

The fate of N atoms contained in the Ponceau SS molecules (0.76 mM) was followed during the PEF treatment at $j = 100$ mA cm^{-2}. Neither NO_2^- nor NO_3^- ions were detected in the degraded solution, whereas 0.34 mM of NH_4^+ (44.7% of initial N) were finally accumulated. These results suggest that the initial N was only mineralized to NH_4^+ ion and, based on the large degree of mineralization reached (93.4%, Table 2), it can be suggested that part of the N was transformed into volatile N-species, like N_2 and N_xO_y, as suggested for other azo dyes.[34,42] From this, the theoretical mineralization reaction for the anionic form of Ponceau SS, with $m = 22$ C atoms and number of electrons $n = 90$, can be expressed as follows:

These are not the final page numbers! ↗↗

Table 2. Apparent rate constant for decolorization with the corresponding R^2, percentage of TOC removal, mineralization current efficiency and energy consumption per unit TOC mass at 360 min of electrolysis of 2.5 L of 0.19 mM Ponceau SS solutions in 0.050 M Na_2SO_4 at pH 3.0 and 35 °C by several EAOPs at different current densities using a pre-pilot flow plant with a cell equipped with a Ti|Pt or BDD anode and an air-diffusion cathode, connected to an annular photoreactor with a 160 W UVA lamp in PEF process.

Method	j [mA cm^{-2}]	k_{dec} [min^{-1}]	R^2	% TOC removal	% MCE	EC_{TOC}[a]
Ti|Pt anode						
AO-H$_2$O$_2$	25	3.7×10^{-3}	0,980	15.0	5.4	1.28
	50	4.3×10^{-3}	0.984	23.9	4.5	2.62
	100	6.0×10^{-3}	0.992	30.8	2.9	5.63
EF	25	1.8×10^{-2}	0.996	42.2	16.1	0.45
	50	2.7×10^{-2}	0.995	51.6	9.8	1.21
	100	5.5×10^{-2}	0.994	60.0	5.7	3.04
PEF	25	1.9×10^{-2}	0.992	72.6	27.6	10.8
	50	3.5×10^{-2}	0.995	87.0	16.6	9.54
	100	6.0×10^{-2}	0.989	93.4	8.9	10.1
BDD anode						
AO-H$_2$O$_2$	25	6.6×10^{-3}	0.982	48.8	18.6	0.64
	50	9.7×10^{-3}	0.990	56.4	10.7	1.10
	100	1.3×10^{-2}	0.981	65.0	6.2	2.74
EF	25	2.3×10^{-2}	0.980	54.2	20.6	0.58
	50	4.4×10^{-2}	0.992	63.0	12.0	1.37
	100	6.5×10^{-2}	0.991	70.6	6.7	3.40
PEF	25	2.6×10^{-2}	0.994	85.2	31.2	9.39
	50	4.6×10^{-2}	0.994	93.8	16.9	9.11
	100	8.7×10^{-2}	0.991	97.6	9.0	10.4

[a] Energy consumption per unit TOC mass [in kWh (g TOC)$^{-1}$] calculated from Eq. (9) for AO-H$_2$O$_2$ and EF and from Eq. (10) for PEF.

$$C_{22}H_{14}N_4O_7S_2{}^{2-} + 45H_2O \rightarrow$$
$$22CO_2 + 2SO_4{}^{2-} + 4NH_4{}^+ + 88H^+ + 90e^- \quad (7)$$
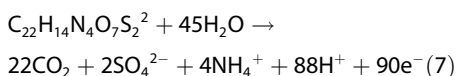
Considering this, the percentage of mineralization current efficiency (MCE) at time t (in h) and applied current I (in A) for each run was calculated from reaction (8):[42]

$$\%MCE = \frac{n\,F\,V\,\Delta(TOC)_{exp}}{4.32\times10^7\,m\,I\,t}\,100 \quad (8)$$

where F is the Faraday constant, V is the solution volume (in L), $\Delta(TOC)_{exp}$ is the TOC removed (in mg L^{-1}) and 4.32×10^7 is a conversion factor ($=3,600$ s h$^{-1}\times12,000$ mg C mol^{-1}).

Figure S1a–c of Supporting Information shows the MCE profiles for the trials of Figure 2a–c. Small efficiencies were obtained in the AO-H$_2$O$_2$ process due to its low mineralization ability. Figure S1a highlights that they were quite similar for j values of 25 and 50 mA cm^{-2}, regularly decreasing for $j=$ 100 mA cm^{-2}. This latter tendency was always observed for all the EF and PEF processes (Figure S1b and c, respectively), which can be ascribed to the progressive loss of organic matter with formation of more recalcitrant by-products.[12] The MCE values listed in Table 2 after 360 min of electrolysis allows inferring that they decreased with increasing j regardless of the method, reaching higher values according to its relative oxidation power. The most efficient treatment was PEF at $j=25$ mA cm^{-2}, with a maximal of 34.1% at 180 min that dropped to 27.6%. The tendency of MCE with increasing j was opposite to that of TOC, since the solution was more rapidly mineralized. This behavior is characteristic of EAOPs due to the larger enhancement of the parasitic (non-oxidizing) reactions of Pt($^\bullet$OH) and $^\bullet$OH that reduce their relative concentration with the consequent loss of MCE[4,15]

Another figure of merit used to confirm the viability of EAOPs is the energy consumption. Based on the $\Delta(TOC)_{exp}$ determined for each run and the corresponding cell voltage (E_{cell}, in V), the energy consumption per unit TOC mass (EC$_{TOC}$, in kWh (g TOC)$^{-1}$) was calculated from Equation (9):[42,43]

$$EC_{TOC} = \frac{E_{cell}\,I\,t}{V\,\Delta(TOC)_{exp}} \quad (9)$$

This equation is valid for AO-H$_2$O$_2$ and EF, as well as for SPEF because of the use of the free natural sunlight. For PEF, however, the electric power of the UVA lamp (160 W in our case) should be added, giving the alternative value of EC$_{TOC,total}$ (kWh (g TOC)$^{-1}$), expressed as follows:

$$EC_{TOC,total} = \frac{(E_{cell}\,I + 160)\,t}{V\,\Delta(TOC)_{exp}} \quad (10)$$

Note that Equation (9) could also be used for PEF, assuming sunlight irradiation, i.e., the potential replacement of the UVA lamp by natural sunlight, as has been well proven experimentally elsewhere.[29,42,43]

As can be seen in Figure S2a and b, the EC$_{TOC}$ values for AO-H$_2$O$_2$ and EF increased with increasing j by the high rise of E_{cell}, the opposite trend to that shown by MCE. This can be also deduced from the data collected in Table 2 at 360 min of both treatments. The lowest EC$_{TOC}$ was achieved in EF at $j=$ 25 mA cm^{-2}, slightly increasing from 0.34 to 0.45 kWh (g TOC)$^{-1}$ during the run. In the case of PEF, Figure S2c shows oscillating values for the enormous EC$_{TOC,total}$ values determined with varying j due to the compensation between the high electrical power of the UVA lamp and the greater TOC removal. They varied between 9.54 and 10.8 kWh (g TOC)$^{-1}$ (Table 2). Never-
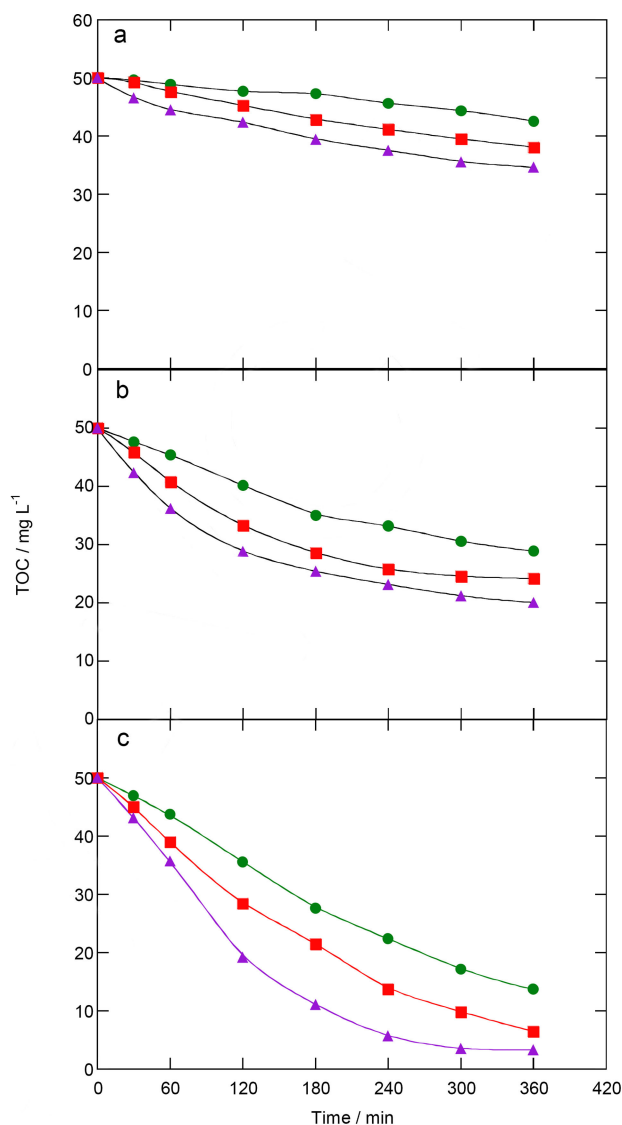
Figure 2. TOC decay with time for the trials of Figure 1 a) AO-H$_2$O$_2$, b) EF, and c) PEF. Current density: 25 (●, green), 50 (■, red), and 100 mA cm^{-2} (▲, violet).

Figure 3. Change of percentage color removal for 2.5 L of 0.19 mM PCSS solution in 0.050 M Na$_2$SO$_4$ at pH 3.0 and 35 °C using a pre-pilot flow plant with a BDD/air-diffusion cell by a) AO-H$_2$O$_2$, b) EF, and c) PEF. Current density: 25 (○, green), 50 (□, red), and 100 mA cm^{-2} (△, violet). The insets present the analysis considering a pseudo-first-order decolorization kinetics.

theless, the corresponding EC$_{TOC}$ values at 360 min assuming no UVA power consumption decreased to 0.29 kWh (g TOC)$^{-1}$ at $j =$ 25 mA cm^{-2} and to 2.09 kWh (g TOC)$^{-1}$ at $j = 100$ mA cm^{-2}, which were much smaller than those obtained in EF. The aforementioned findings demonstrate a greater ability of PEF process to decolorize and mineralize the Ponceau SS solution as a result of the action of UVA radiation upon the photoactive intermediates originated by the attack of Pt(•OH) and •OH.

2.2. Degradation of Ponceau SS using a BDD Anode

The study of the decolorization and mineralization of 2.5 L of 0.19 mM Ponceau SS solutions in 0.050 M Na$_2$SO$_4$ at pH 3.0 was extended to a BDD/air-diffusion cell in the pre-pilot flow plant under comparable conditions to those used with Pt. EF and PEF

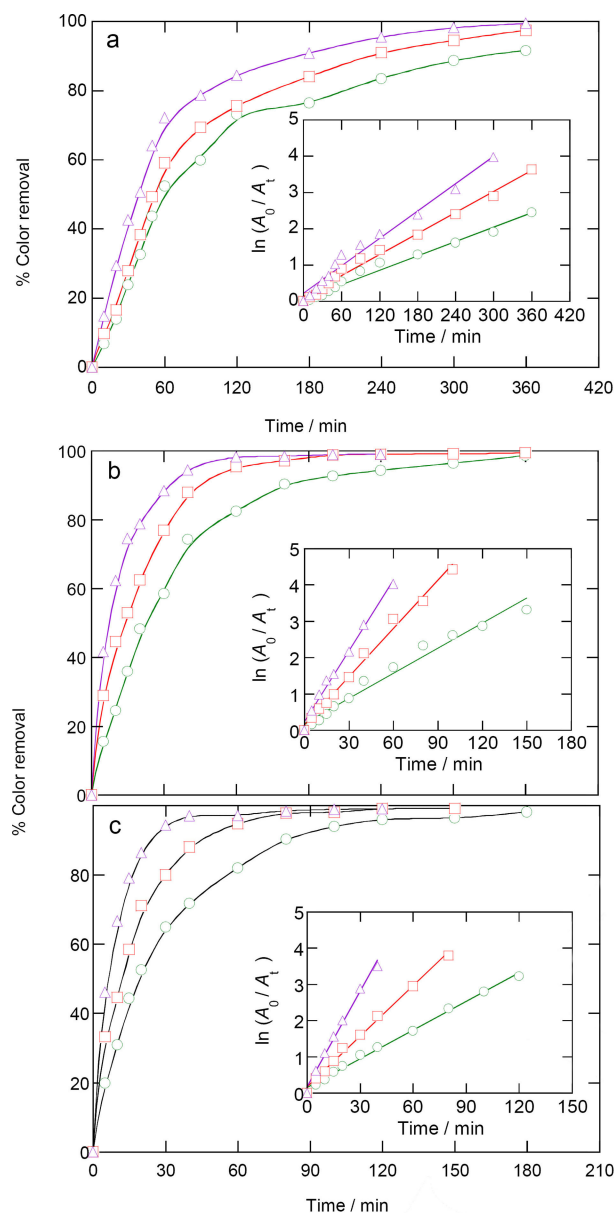were made with 0.50 mM Fe^{2+}. A slight decrease of the initial pH down to 2.6–2.7 was also found after 360 min.

Figure 3a–c illustrates the variation of color removal during the treatments carried out with a BDD anode. A progressively greater loss of color at higher j can be observed for each method, associated with the concomitant larger generation of BDD(•OH) and/or •OH due to the increase in rate of reactions (1)–(3). The diazo dye solution was also decolorized much more quickly by EF and PEF compared to AO-H$_2$O$_2$, thereby demonstrating the large oxidation enhancement of the target molecule and its colored products by •OH in the bulk. The insets of Figure 3a–c show the excellent linear relationships

These are not the final page numbers! ↗↗

obtained from a pseudo-first-order analysis of the corresponding absorbance drops. As expected, the resulting k_{dec}-values, listed in Table 2, increased with increasing j for each EAOP. Moreover, comparison of these constants confirmed a raising decolorization power in the order: AO-$H_2O_2 \ll$ EF < PEF. Worth mentioning, the upgrade in •OH production from photolytic reaction (4) accounts for the decolorization enhancement in PEF compared to EF. On the other hand, an inspection of Table 2 allows inferring the greater k_{dec}-values found in all cases with BDD compared to those obtained with Pt. While k_{dec} was 1.8–2.2 fold higher in AO-H_2O_2, it underwent a smaller grew of 1.2–1.5-fold in EF and PEF. The remarkable rise in decolorization rate in the former EAOP using a non-active BDD anode agrees with the expected greater oxidation ability of BDD(•OH).[4,12,31] The parallel effective oxidation with •OH explains the smaller contribution of the above physisorbed radicals in the two Fenton-based EAOPs.

The TOC-time plots depicted in Figure 4a–c using a BDD anode, along with the percentage of TOC removal given in Table 2, evidence a faster mineralization in the sequence: AO-$H_2O_2 <$ EF < PEF. This is in agreement with the decolorization behavior pointed out above and the results obtained with a Ti | Pt anode. This corroborates the increasing role of BDD(•OH), •OH and UVA light to destroy organic pollutants leading to the above relative oxidation power of EAOPs. Figure 4a–c and Table 2 also confirm the greater mineralization achieved for each method when j was increased from 25 to 100 mA cm^{-2}, as expected by the larger production of reactive BDD(•OH) and/or •OH. It is remarkable the considerable growth of mineralization in AO-H_2O_2 when using BDD instead of Pt; for example, 65.0% vs. 30.8% TOC reduction at 360 min of $j = 100$ mA cm^{-2} (Table 2). This difference was less significant in EF (70.6% vs. 60.0%) due to the important oxidation via •OH in the bulk, and only a minimum difference was found in PEF (97.6% vs. 93.4%) as a result of UVA irradiation.

These findings point to a clear superiority of BDD to be used in the AO-H_2O_2 and EF treatment of Ponceau SS solutions, being much less evident in PEF, particularly at high j values, where a large mineralization with > 93% TOC abatement can be reached (Figure 2c and 4c).

The MCE values at 360 min (Table 2) showed a gradual drop with increasing j for each EAOP, as expected by the progressive larger extent of the parasitic reactions.[14,15,42] The relative oxidation ability of BDD anode grew in the order: AO-$H_2O_2 <$ EF < PEF, as for Pt. Comparison of the MCE data for both anodes confirms the much higher efficiency achieved using the former anode in AO-H_2O_2 (e.g., 6.2% vs. 2.9% at 100 mA cm^{-2}). This difference was strongly reduced in EF (6.7% vs. 5.7% at the same j), whereas in PEF, the same mineralization current efficiencies were practically obtained at 50 mA cm^{-2} (16.6%–16.9%) and 100 mA cm^{-2} (8.9–9.0%). Regarding the EC$_{TOC}$ values in AO-H_2O_2 and EF with BDD of Table 2, they increased with j and were significantly lower than those obtained with Pt, despite the higher E_{cell} of the BDD/air-diffusion cell due to the larger mineralization reached. In contrast, the EC$_{TOC,total}$ values determined in PEF varied between 9.1 and 10.4 kWh (g TOC)$^{-1}$, quite analogous to those found for Pt because of the very large contribution of the lamp power. When this contribution was
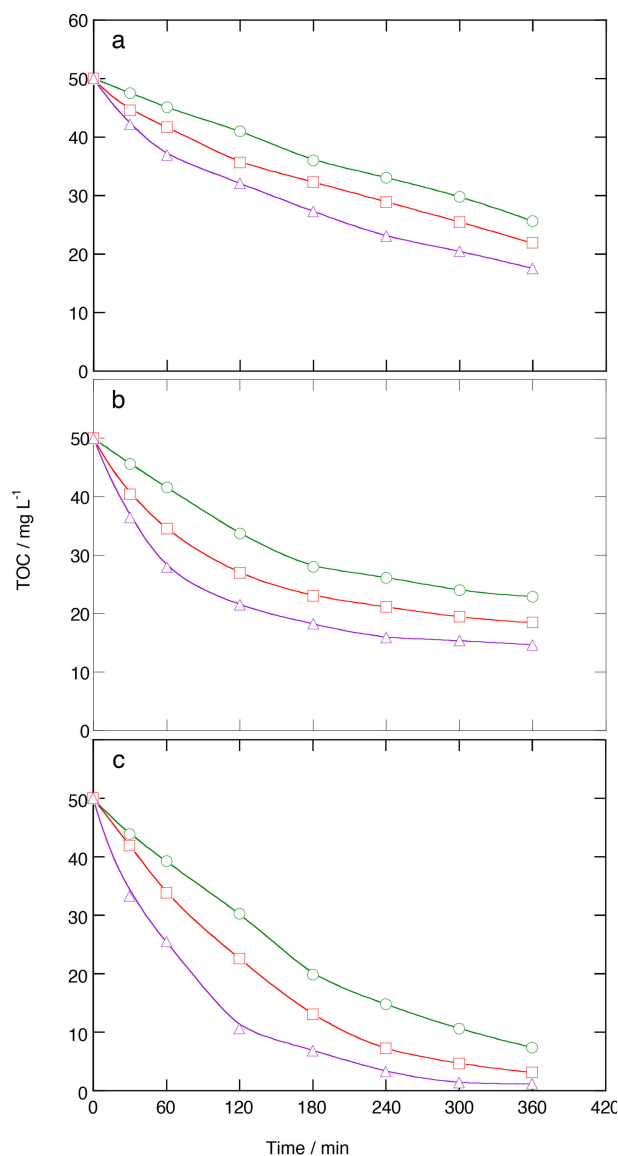

Figure 4. TOC abatement for the assays of Figure 3 a) AO-H_2O_2, b) EF, and c) PEF. Current density: 25 (○, green), 50 (□, red), and 100 mA cm^{-2} (△, violet).

not considered, the EC$_{TOC}$ values were 0.37, 0.97, and 2.46 kWh (g TOC)$^{-1}$ at 25, 50, and 100 mA cm^{-2}, respectively, which are much greater than in the case of Pt (see section 2.1).

The study performed for the degradation of Ponceau SS in the pre-pilot flow plant with a cell containing an air-diffusion electrode indicates that the BDD anode is preferable in AO-H_2O_2 and EF, because it provides faster decolorization and TOC reduction, with higher MCE and lower EC$_{TOC}$. Under PEF conditions at $j \geq 50$ mA cm^{-2}, however, both anodes showed a quite similar degradation performance.

2.3. Detection of Oxidation Products using a Pt Anode

Five primary aromatic products formed during the PEF degradation of a 0.19 mM Ponceau SS solution in the pre-pilot plant with a Ti | Pt anode at $j = 50$ mA cm^{-2} were identified by

These are not the final page numbers! ↗↗

GC-MS. They were 2 azo derivatives and 3 benzenic products, which were also found in AO-H_2O_2 and EF, as well as in all EAOPs using BDD, since they arise from the attack of hydroxyl radicals (generated in all cases) onto the initial dye. On this basis, Scheme 1 proposes a reaction sequence for the primary
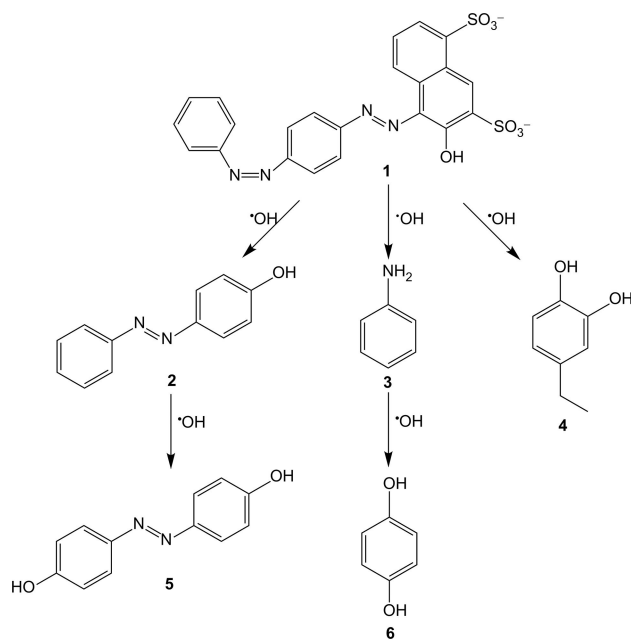
Scheme 1. Proposed initial route for the degradation of Ponceau SS diazo dye by EAOPs. $^{\bullet}$OH represents the hydroxyl radical formed at the anode surface from water oxidation and in the bulk from Fenton's reaction.

degradation of Ponceau SS (**1**) involving such radicals as main oxidants. This pathway highlights that the initial hydroxylation of **1** leads to the cleavage of either one azo group leading to 4-(phenylazo)phenol (**2**) and aniline (**3**), or part of its naphthalenic ring originating 4-ethyl-1,2-benzenediol (**4**). Further hydroxylation of **2** yields the hydroxylated di-(4-hydroxy-phenyl)diazene (**5**), whereas that of **3** gives hydroquinone (**6**).

It is well known that the subsequent destruction of the above aromatics leads to short-chain aliphatic carboxylic acids, which form Fe(III) complexes under PEF conditions.[41–45] A mixture of oxalic, tartronic, malic, and acetic acids was detected for the above assay by ion-exclusion HPLC. Figure 5 illustrates the evolution of these acids during the treatment. Total removal of Fe(III)-oxalate, Fe(III)-tartronate and Fe(III)-acetate complexes was achieved at the end of the electrolysis, pre-eminently due to their photolysis via reaction (5) since such Fe(III)-carboxylate were very poorly abated by Pt($^{\bullet}$OH) and $^{\bullet}$OH.[14,15] In contrast, Fe(III)-malate complexes were more slowly degraded and 13.0 mg L^{-1} of malic acid remained in the final solution, representing 3.5 mg L^{-1} TOC that corresponds to 26.9% of the organic load (13.0 mg L^{-1} as deduced from Table 2). This can be explained by the formation of a larger proportion of other recalcitrant undetected products that can be more rapidly removed by increasing j or using a BDD anode because of the higher oxidation power of BDD($^{\bullet}$OH).
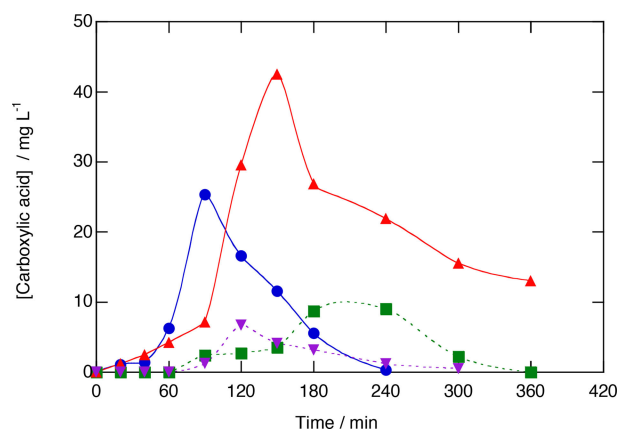

Figure 5. Time-course of the concentration of oxalic (●, blue), tartronic (■, green), malic (▲, red), and acetic (▼, violet) acids detected during the PEF degradation of 2.5 L of 0.19 mM Ponceau SS solution in 0.050 M Na$_2$SO$_4$ at pH 3.0 using a pre-pilot flow plant with a Pt/air-diffusion cell at 50 mA cm^{-2},

3 Conclusions

It has been shown that 2.5 L of a 0.19 mM Ponceau SS solution in acidic sulfate medium treated a pre-pilot flow plant by AO-H_2O_2 and EF were more quickly decolorized and mineralized using a BDD/air-diffusion cell. This is due to the much greater oxidation ability of BDD($^{\bullet}$OH) compared to Pt($^{\bullet}$OH), partially compensated by the parallel oxidation by $^{\bullet}$OH produced from Fenton's reaction in EF. PEF was the most powerful EAOP thanks to the additional potent photolytic action of UVA radiation, leading to a quite similar decolorization and mineralization rate for both cells. In all cases, the decolorization decay obeyed a pseudo-first-order kinetics, with increasing k_{dec}-values with raising j. The same trend was found for TOC abatement, with loss of mineralization current efficiency and increase of the energy consumption. High EC$_{TOC,total}$ values were obtained in PEF taking into account the lamp power, but the corresponding consumption if lamp power was not considered was lower than those of AO-H_2O_2 and EF. The use of an active anode to destroy the diazo dye by photo-assisted Fenton-based EAOPs is thus recommended, whereas the non-active BDD results more useful in AO-H_2O_2 and EF. Five primary aromatic products and four final carboxylic acids were detected.

Experimental Section

Ponceau SS (80% purity, and the rest of components were stabilizing salts) was purchased from Sigma-Aldrich. Sulfuric acid (96% purity) from Acros Organics and analytical grade NaOH from Panreac were used to adjust pH conditions. All the solutions were prepared with deionized water. The rest of chemicals including Na$_2$SO$_4$ and FeSO$_4 \cdot$7H$_2$O used as background electrolyte and catalyst, respectively, were of analytical or HPLC grade purchased from Fluka, Merck, Panreac and Sigma-Aldrich.

Electrochemical assays were carried out in a 2.5 L pre-pilot flow plant composed of the following consecutive elements:[45] (i) a PVC reservoir containing the solution; (ii) a centrifugal pump to recirculate the solution through the system; (iii) a rotameter to

regulate the liquid flow rate at 200 L h^{-1}; (iv) two heat exchangers to maintain the solution temperature at 35 °C; (v) a filter-press electrochemical cell equipped with a BDD thin-film on Si (NeoCoat) or a Ti | Pt (NMT) anode and a carbon-PTFE air-diffusion cathode (Sainergy Fuel Cell), all with 20 cm^2 of geometric area in contact with the solution and separated 1.2 cm; and (vi) an annular Schott-Duran glass photoreactor containing 640 mL of solution volume. Atmospheric air at overpressure of 8.6 kPa was injected to the dry face of the cathode for H_2O_2 production. The plant was covered with an opaque cloth for AO-H_2O_2 and EF trials, whereas a Philips 160 W UVA lamp ($\lambda_{max} = 360$ nm) was centered in the annular photoreactor for PEF. Galvanostatic electrolyses were performed with a Grelco GVD310 (0–10 A) power supply, which displayed directly the cell voltage (E_{cell}).

A Crison GLP22 pH-meter was used to measure the pH of solutions. Prior to analysis, all the samples were filtered with Whatman 0.45 μm PTFE filters. In EF and PEF, they were previously alkalinized to stop the degradation. The loss of solution color was determined from the absorbance decay at $\lambda_{max} = 514$ nm using a Shimadzu 1800 UV/vis spectrophotometer. The same equipment was utilized for the determination of H_2O_2 from its Ti(IV) complex.[46] TOC was measured on a Shimadzu TOC-VCSN analyzer, by injecting 50 μL aliquots and with a precision of ±1%. Average values (±2% values) are reported for replicated decolorization and TOC measurements.

Ion-exclusion HPLC analysis was performed by injecting 10 μL into a Waters system (600 LC and 996 photodiode array detector at $\lambda = 210$ nm) using an Aminex HPX 87H, 300 mm × 7.8 mm, column at 35 °C from Bio-Rad and eluting 4 mM H_2SO_4 solution at 0.6 mL min^{-1}. Retention times of 6.7, 7.7, 9.6 and 15.2 min for oxalic, tartronic, malic and acetic acids, respectively, were found. NH_4^+ concentration was obtained from the standard phenate method.[47] GC-MS analysis was made after extraction with CH_2Cl_2 (3×25 mL) of the organic components of 100 mL of solutions treated during short times by PEF using a Pt/air-diffusion cell, followed by drying the resulting organic solution with Na_2SO_4, filtration and volume reduction. An Agilent system with a non-polar J&W HP-5 ms 0.25 μm, 30 m×0.25 mm, column, was utilized as reported previously.[30] The products were identified with the help of a NIST05 MS library.

Acknowledgements

Conflict of Interest

The authors declare no conflict of interest.

References

[1] T. Robinson, G. McMullan, R. Marchant, P. Nigam, *Biores. Technol.* **2001**, *77*, 247–255.

[2] H. Zollinger, *Color Chemistry: Synthesis, Properties, and Applications of Organic Dyes and Pigments*, VHCA and Wiley-VCH, Switzerland, **2003**.

[3] V. Khandegar, A. K. Saroha, *J. Environ. Manage.* **2013**, *128*, 949–963.

[4] E. Brillas, C. A. Martínez-Huitle, *Appl. Catal. B: Environ.* **2015**, *166–167*, 603–643.

[5] UNESCO, *The United Nations World Water Development Report 4, Vol. 1: Managing Water Report under Uncertainty and Risk*, **2012**.

[6] E. Forgacs, T. Cserháti, G. Oros, *Environ. Int.* **2004**, *30*, 953–971.

[7] A. B. dos Santos, F. J. Cervantes, J. B. van Lier, *Biores. Technol.* **2007**, *98*, 2369–2385.

[8] S. M. A. G. Ulson de Souza, E. Forgiarini, A. A. Ulson de Souza, *J. Hazard. Mater.* **2007**, *147*, 1073–1078.

[9] K. P. Sharma, S. Sharma, S. P. Sharma, K. Singh, S. Kumar, R. Grover, P. K. Sharma, *Chemosphere* **2007**, *69*, 48–54.

[10] R. Sanghi, B. Bhattacharya, *Water Qual. Res. J. Can.* **2003**, *38*, 553–562.

[11] A. K. Verma, R. R. Dash, P. Bhunia, *J. Environ. Manage.* **2012**, *93*, 154–168.

[12] M. Panizza, G. Cerisola, *Chem. Rev.* **2009**, *109*, 6541–6569.

[13] A. Anglada, A. Urtiaga, I. Ortiz, *J. Chem. Technol. Biotechnol.* **2009**, *84*, 1747–1755.

[14] I. Sirés, E. Brillas, *Environ. Int.* **2012**, *40*, 212–229.

[15] I. Sirés, E. Brillas, M. A. Oturan, M. A. Rodrigo, M. Panizza, *Environ. Sci. Pollut. Res.* **2014**, *21*, 8336–8367.

[16] E. Tsantaki, T. Velegraki, A. Katsaounis, D. Mantzavinos, *J. Hazard. Mater.* **2012**, *207–208*, 91–96.

[17] M. B. Ferreira, J. H. B. Rocha, J. V. de Melo, C. A. Martínez-Huitle, M. A. Quiroz Alfaro, *Electrocatalysis* **2013**, *4*, 274–282.

[18] M. A. Quiroz, J. L. Sánchez-Salas, S. Reyna, E. R. Bandala, J. M. Peralta-Hernández, C. A. Martínez-Huitle, *J. Hazard. Mater.* **2014**, *268*, 6–13.

[19] A. Thiam, I. Sirés, J. A. Garrido, R. M. Rodríguez, E. Brillas, *Sep. Purif. Technol.* **2015**, *140*, 43–52.

[20] M. Rivera, M. Pazos, M. A. Sanromán, *Desalination* **2011**, *274*, 39–43.

[21] M. Panizza, M. A. Oturan, *Electrochim. Acta* **2011**, *56*, 7084–7087.

[22] N. Daneshvar, S. Aber, V. Vatanpour, M. H. Rasoulifard, *J. Electroanal. Chem.* **2008**, *615*, 165–174.

[23] M. S. Yahya, N. Oturan, K. El Kacemi, M. El Karbane, C. T. Aravindakumar, M. A. Oturan, *Chemosphere* **2014**, *117*, 447–454.

[24] F. Sopaj, M. A. Rodrigo, N. Oturan, F. I. Podvorica, J. Pinson, M. A. Oturan, *Chem. Eng. J.* **2015**, *262*, 286–294.

[25] P. A. Diaw, N. Oturan, M. D. Gaye-Seye, A. Coly, A. Tine, J.-J. Aaron, M. A. Oturan, *Sep. Purif. Technol.* **2017**, *186*, 197–206.

[26] A. Khataee, A. Khataee, M. Fathinia, B. Vahid, S. W. Joo, *J. Ind. Eng. Chem.* **2013**, *19*, 1890–1894.

[27] A. Khataee, A. Akbarpour, B. Vahid, *J. Taiwan Inst. Chem. Eng.* **2014**, *45*, 930–936.

[28] X. Florenza, A. M. S. Solano, F. Centellas, C. A. Martínez-Huitle, E. Brillas, S. Garcia-Segura, *Electrochim. Acta* **2014**, *142*, 276–288.

[29] A. Thiam, I. Sirés, F. Centellas, P. L. Cabot, E. Brillas, *Chemosphere* **2015**, *136*, 1–8.

[30] J. R. Steter, E. Brillas, I. Sirés, *Electrochim. Acta* **2016**, *222*, 1464–1474.

[31] B. Marselli, J. García-Gomez, P. A. Michaud, M. A. Rodrigo, C. Comninellis, *J. Electrochem. Soc.* **2003**, *150*, D79-D83.

[32] A. Kapałka, G. Fóti, C. Comninellis, *Electrochim. Acta* **2009**, *54*, 2018–2023.

[33] J. H. Bezerra Rocha, M. M. Soares Gomes, E. Vieira dos Santos, E. C. Martins de Moura, D. Ribeiro da Silva, M. A. Quiroz, C. A. Martínez-Huitle, *Electrochim. Acta* **2014**, *140*, 419–426.

[34] S. Garcia-Segura, F. Centellas, C. Arias, J. A. Garrido, R. M. Rodríguez, P. L. Cabot, E. Brillas, *Electrochim. Acta* **2011**, *58*, 303–311.

[35] A. Bedolla-Guzman, I. Sirés, A. Thiam, J. M. Peralta-Hernández. S. Gutiérrez-Granados, E. Brillas, *Electrochim. Acta* **2016**, *206*, 307–316.

[36] K. Cruz-González, O. Torres-López, A. García-León, J. L. Guzmán-Mar, L. H. Reyes, A. Hernández-Ramírez, J. M. Peralta-Hernández, *Chem. Eng. J.* **2010**, *160*, 199–206.

[37] L. Feng, E. D. Van Hullebusch, M. A. Rodrigo, G. Esposito, M. A. Oturan, *Chem. Eng. J.* **2013**, *228*, 944–964.

[38] M. A. Oturan, J.-J. Aaron, *Crit. Rev. Environ. Sci. Technol.* **2014**, *23*, 2577–2641.

[39] A. Wang, J. Qu, H. Liu, J. Ru, *Appl. Catal. B: Environ.* **2008**, *84*, 393–399.

[40] V. S. Antonin, S. Garcia-Segura, M. C. Santos, E. Brillas, *J. Electroanal. Chem.* **2015**, *747*, 1–11.

These are not the final page numbers! ↗↗

[41] A. M. S. Solano, C. A. Martínez-Huitle, S. Garcia-Segura, A. El-Ghenymy, E. Brillas, *Electrochim. Acta* **2016**, *197*, 210–220.

[42] E. J. Ruiz, A. Hernández-Ramírez, J. M. Peralta-Hernández, C. Arias, E. Brillas, *Chem. Eng. J.* **2011**, *171*, 385–392

[43] F. C. Moreira, S. Garcia-Segura, V. J. P. Vilar, R. A. R. Boaventura, E. Brillas, *Appl. Catal. B: Environ.* **2013**, *142–143*, 877–890.

[44] G. Coria, I. Sirés, E. Brillas, J. L. Nava, *Chem. Eng. J.* **2016**, *304*, 817–825.

[45] C. Flox, J. A. Garrido, R. M. Rodríguez, P. L. Cabot, F. Centellas, C. Arias, E. Brillas, *Catal. Today* **2007**, *127*, 29–36.

[46] F. J. Welcher, *Standard Methods of Chemical Analysis, 6th ed, Vol.* 2, Part B, R. E. Krieger Publishing Co, Huntington, New York, **1975**.

[47] A. D. Eaton, L. S. Clesceri, A. E. Greenberg, *Standard Methods for the Examination of Water and Wastewater*, 22nd ed, APHA, AWWA, WEF, **2012**.

ARTICLES

Degradation of Ponceau SS dye:
Similar decolorization and mineralization rates are obtained with photo-electro-Fenton by using a pre-pilot flow plant with a BDD/air-difffusion or Pt/air-diffusion cell. Initially, five aromatic products are formed, followed by their conversion into four carboxylic acids, which are transformed into carbon dioxide (see figure).
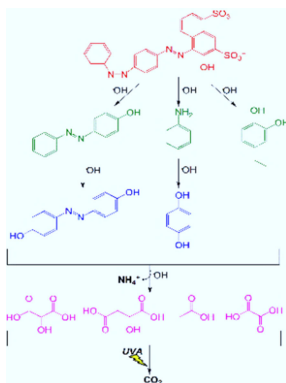
A. J. dos Santos, Prof. C. A. Martínez-Huitle, Prof. I. Sirés, Prof. E. Brillas*

1 – 10

Use of Pt and Boron-Doped Diamond Anodes in the Electrochemical Advanced Oxidation of Ponceau SS Diazo Dye in Acidic Sulfate Medium